Sea ice formation in a coupled climate model including grease ice

Shona Mackie[1], Patricia J. Langhorne[1], Harold D. B. S. Heorton[2], Inga J. Smith[1], Daniel L. Feltham[3], David Schroeder[3]

[1]Department of Physics, University of Otago, 730 Cumberland Street, Dunedin 9016, New Zealand
[2]Department of Earth Science, University College London, Gower Street, London WC1E 6BT, United Kingdom
[3]Department of Meteorology, University of Reading, Reading RG6 6AH, United Kingdom

Key Points:

- A more detailed representation of sea ice formation is implemented in a coupled climate model ensemble
- Including grease ice processes results in increased Arctic sea ice thickness and volume
- Including grease ice processes results in large local changes to Antarctic winter sea ice concentration and thickness

Corresponding author: Shona Mackie, shonalmackie@gmail.com

Abstract

Sea ice formation processes occur on sub-grid scales and the detailed physics describing the processes are therefore not generally represented in climate models. One likely consequence of this is the premature closing of areas of open water in model simulations, which may result in a misrepresentation of heat and gas exchange between the ocean and atmosphere. This work demonstrates the implementation of a more realistic model of sea ice formation, introducing grease ice as a wind- and oceanic- stress-dependant intermediary state between water and new sea ice. We use the fully coupled land-atmosphere-ocean- sea ice model, HadGEM3-GC3.1 and perform a three member ensemble with the new grease ice scheme from 1964 to 2014. Comparing our sea ice results with the existing ensemble without grease ice formation shows an increase in sea ice thickness and volume in the Arctic. In the Antarctic, including grease ice processes results in large local changes to both simulated sea ice concentration and thickness, but no change to the total area or volume.

Plain Language Summary

The way that new sea ice forms in most climate models may result in new sea ice forming more quickly than it does in reality, prematurely closing areas of open water that are important to heat and gas exchange between the ocean and atmosphere, and impacting the albedo, and therefore the radiation budget, of the planet. In this work, we implement a more realistic representation of how new sea ice forms in a fully coupled climate model, and demonstrate the effect using an ensemble of historical climate simulations.

1 Introduction

Large scale climate models struggle to accurately calculate Arctic sea ice volume (Shu et al., 2015) and thickness (Stroeve et al., 2014; Langehaug et al., 2013), and to capture trends in Antarctic sea ice extent (Turner et al., 2013). Various processes represented in the models have been investigated to explain this, including natural variability (Zunz et al., 2013), winds (Holland & Kwok, 2012) and melting ice shelves (Pauling et al., 2017). The latest generation of climate models include a more detailed representation of sea ice processes, (Ridley et al., 2018), and here we build on those advances by implementing a more sophisticated representation of sub-grid scale sea ice formation processes in historical climate simulations.

An important mode of sea ice formation results from supercooling of ocean water. Where the temperature of ocean water is lower than its salinity-dependant freezing temperature, the water is supercooled and frazil crystals may form. These small buoyant ice crystals rise to the surface and may either freeze to the underside of existing sea ice, or mix with surface waters to form a slushy mix referred to as grease ice. Supercooling may arise in response to river drainage or the mixing of ocean masses with different salinities (Martin & Kauffman, 1981). More commonly, it follows from a buoyant freshwater flux at depth, for example beneath Antarctic ice shelves (Lewis & Perkin, 1986, 1983), or in response to extreme atmospheric surface cooling, for example in leads and polynyas, where frazil created at the surface is mixed downwards by wind-generated turbulence (Morales Maqueda et al., 2004). Polynyas are holes in the sea ice (or areas where ice does not form), created primarily by either strong offshore winds or by the creation of "hot spots" driven by warm waters upwelling or, in the Arctic, by solar heating (Morales Maqueda et al., 2004), while leads are fractures in sea ice caused by internal stresses. It is possible for snow to be blown from the sea ice surface into areas of open water, creating a slush that is distinguishable from a frazil-formed layer of grease ice only through isotope analysis in a laboratory (Weeks, 2010; Smedsrud & Skogseth, 2006).

At present, most climate models remove supercooling from the surface of the ocean by transforming the energy deficit to a volume of new ice using the latent heat of freezing for ice (e.g., The Los Alamos National Laboraory sea ice model, CICE (Hunke et al., 2015)). This means that no grease ice is created and new sea ice forms instantly in response to supercooling at the surface. In reality, grease ice may persist for several days before atmospheric cooling causes the water fraction to solidify to create sea ice (Smedsrud & Skogseth, 2006). Exposure to a warm atmosphere may cause the solid fraction to melt and the grease ice may reduce, or disappear altogether without ever forming new sea ice. This could mean that sea ice in climate models forms too fast, and areas of open water may close more quickly in the models than is appropriate. Where grease ice forms close to sea ice in the real world, the grease ice may be 'herded' against the sea ice edge by atmospheric and oceanic stress, leading to an uneven grease ice thickness distribution, and sometimes leaving part of the water area free from grease ice (Smedsrud, 2011; Skogseth et al., 2009; Smedsrud & Skogseth, 2006; Martin & Kauffman, 1981). This herding effect cannot be represented without grease ice being represented in the model, and omitting it could contribute further to the premature freezing over of leads and polynyas, and result in new sea ice created in the model being too thin.

Heat and gas exchange between the polar ocean and atmosphere generally serves to cool the upper ocean and warm the lower atmosphere (Morales Maqueda et al., 2004), and is inhibited by sea ice cover, meaning that polynyas and leads directly affect ocean-atmosphere heat and carbon dioxide cycles. In addition, polynyas and leads represent dark holes in the relatively reflective sea ice, impacting albedo, and therefore the planetary radiation budget. Open water areas are also important for plankton (Arrigo et al., 1999) and macrofauna (Stirling, 1997), meaning that the importance of appropriately representing leads and polynyas will increase further as Earth System Models increase in complexity to include more biological processes. In the Antarctic, coastal polynyas are a major source of sea ice production as extreme atmospheric cooling and strong offshore winds drive supercooling and the formation of grease ice, which is driven away from the coast by the strong winds, solidifying into new sea ice (which is also transported by the wind) and exposing the polynya surface water to further cooling (Morales Maqueda et al., 2004). Appropriate representation of polynyas is therefore important for a realistic representation of sea ice formation.

A coupled climate model includes wider atmospheric and oceanic processes that are likely to largely determine the volume of sea ice produced in the model, and biases in these are likely to dominate over any biases in the detailed sea ice formation calculations. However, a more physically realistic representation of sea ice formation ensures that the location and rate of sea ice growth are more realistic. Few field observations are available for grease ice because of the logistical difficulties of reaching and working in areas where it forms. This paucity of data on which to base any parameterisation is partly why grease ice processes are generally not represented in large scale global climate models. Another reason is the computational expense of including subgrid scale processes in a relatively coarse global model. Despite these challenges, a parameterization has been proposed to represent grease ice processes within leads in large scale models (Smedsrud, 2011). The method has been demonstrated for partially ice-covered cells in a sea ice model (Wilchinsky et al., 2015), and in a coupled sea ice-ocean model (Smedsrud & Martin, 2015). Here, we extend those works to include a representation of grease ice processes in grid cells that are either fully or partially ice-free in the coupled land-atmosphere-ocean-sea ice model, HadGEM3-GC3.1. We assess the effect of implementing the grease scheme on the model sea ice concentration and thickness, using an ensemble of historical simulations from 1964 to 2013, and use data derived from observations for the latter part of the same period as reference where possible.

2 Model Description

The new scheme is implemented in the coupled atmosphere-land-ocean-sea ice model, HadGEM3-GC3.1, the physical core of the UK and New Zealand Earth System Models(Kuhlbrodt et al., 2018; Williams et al., 2017). For the ocean component, GO6 (based on NEMO3.6 (Madec & team, 2016)), see Storkey et al. (2018), and for the sea ice component, GSI8.1 (based CICE5.1 (Hunke et al., 2015)), see Ridley et al. (2018). The atmosphere component is provided by the Unified Model, using the GA7.1 configuration, and the land component is the JULES model, configured as GL7.1 (Walters et al., 2019). The ORCA1 grid (nominally 1° resolution) was used for the sea ice and ocean, with 75 vertical ocean layers, and the atmosphere model was run at 1.875° by 1.25° resolution, with 85 vertical levels. Simulations were implemented on the global domain.

In the model, sea ice is assigned to one of five thickness categories, and may move to a different category as it thins or thickens. Sea ice belonging to different categories can co-exist in the same grid cell, and the sum of the concentration for the different categories gives the total ice concentration for the cell (ice concentration is the fraction of the grid cell covered by sea ice). In the standard scheme, if the ocean surface temperature is below its salinity-dependant freezing temperature, new sea ice forms. The amount of supercooling is transformed to an equivalent ice volume using the latent heat of freezing for ice. If there is no open water in the cell, then the new ice volume freezes to the existing sea ice, proportioned between the different ice categories according to their relative concentrations in the cell. If there is open water in the cell, then the new ice volume forms a layer new sea ice of uniform thickness over the open water portion of the cell, with a minimum thickness of 5 cm, and a maximum thickness of 60 cm (the minimum thickness requirement means that it may only partially fill the open water part of the cell). If the volume of new ice is greater than can be accommodated in the open water part of the cell, then the water fraction is covered with 60 cm thick new sea ice, and the remaining new ice is distributed between the categories of existing sea ice.

3 Grease Scheme

The new scheme is outlined in Figure 1. The surface ocean freeze-melt potential is converted to an ice volume as in the standard model. If the cell is ice covered, the new ice volume freezes to, and thickens, the existing sea ice as in the standard scheme. If there is any open water in the cell, then the magnitude of the combined wind and ocean stress is calculated. If the net stress is zero, then no grease ice forms, and the new ice volume constitutes new sea ice, which forms an evenly thick layer over the open water part of the cell as in the standard scheme (this form of new sea ice is continuous, thin, flexible nilas, which has been observed for example by Smedsrud and Skogseth (2006); Winsor and Björk (2000)). If the stress magnitude is greater than zero, and there is open water present, then we implement the grease scheme. Under the grease scheme, the new ice volume is not immediately considered to be new sea ice. Instead, some of it constitutes a volume of frazil ice, which makes up the solid fraction of a layer of grease ice in the open water part of the cell, comprised of 25% frazil and 75% sea water (following the convention set by previous model studies (Heorton et al., 2017; Wilchinsky et al., 2015; Smedsrud & Martin, 2015)). If there is grease ice in the cell persisting from the previous time step, then this is added to the new grease ice volume. Note that, for the purposes of this work, 'grease ice' is distinct from 'sea ice' and does not contribute to the values for sea ice concentration or volume (unless/until it freezes to become new sea ice, at which point it is no longer considered to be grease ice). We continue to refer to the open water fraction of a grid cell as open water, regardless of whether the water contains grease ice or not, i.e., the sea ice concentration and water concentration sum to unity. Note also that although the volume of grease ice is preserved between timesteps, the concentration and thickness of the grease are recalculated each timestep.

In most cases, supercooling giving rise to frazil formation is driven by atmospheric cooling, and so it may be reasonable to assume that frazil produced in a partially ice-covered cell is concentrated in the open water fraction of the cell. However, it is also possible for supercooling to result from mixing of waters with different salinities, e.g., where ocean masses meet, or where rivers or ice shelf melt provide freshwater fluxes (Martin & Kauffman, 1981). In these cases, it is unrealistic for all the frazil created in a cell to be concentrated in the open water, and in some cases this assumption could lead to problems. For example, if sea ice concentration is high, then forcing all frazil to be concentrated in a relatively small area of open water could lead to the formation of an unrealistically thick grease ice layer. Therefore, in partially ice-covered cells, not all of the frazil produced from surface supercooling is used to create grease ice. Instead, grease ice is created from only a proportion of the total frazil that is equal to the cell open water concentration. The remainder of the frazil thickens the existing sea ice (for ice-free cells, all frazil produced in the cell becomes part of the grease ice). Ideally, the origin of the supercooling (and hence of the frazil) would be determined from other model parameters and used to determine whether the frazil should be concentrated in the open water or not. For example a full mixed layer model could be used to create frazil crystals in the water column, as demonstrated in Wilchinsky et al. (2015), however that mixed layer model was not compatible with a coupled ocean model. The scheme presented here represents an improvement over the standard configuration (where no grease ice forms at all) but may underestimate the volume of grease ice in many cases.

3.1 Grease Concentration and Thickness

For ice-free cells, the grease ice volume, V_g, is distributed evenly over the cell, giving grease ice concentration $C_g = 1$, and grease thickness $H_g = V_g/C_g$ (grease ice concentration is the fraction of the grid cell area covered by grease ice). Since the surface area covered by a grid cell varies at high latitudes in the ORCA tripolar grid, calculations in the sea ice model are carried out with respect to concentration (which is unitless) rather than area. As the product of concentration and depth, volume, as calculated in the model, therefore has units of meters, and the grid cell area is generally used in post processing and analysis to convert this to cubic meters.

For partially ice-covered cells, all open water is assumed to represent leads in the sea ice. A lead-sea ice element is conceptualized as extending the full length of the cell, with width Y, made of sea ice width L_i and lead width L_l, see Figure 2a, where H_i and H_g are the sea ice and grease ice thicknesses respectively. The grease ice has span L_g, which may not equal L_l if conditions are conducive to herding as described below. Sea ice in each thickness category that is present in the cell makes up the lead walls for a fraction of the lead length proportional to that category's relative concentration, see Figure 2b. We set the width of the lead-sea ice element, $Y = 5$ km, sea ice width, $L_i = YC_i$ and lead width, $L_l = Y - L_i$, following Wilchinsky et al. (2015) (C_i is ice concentration). This means that for a cell with $C_i = 0.9$, $L_l = 500$ m.

3.1.1 No Herding

If there is insufficient open water to create leads of at least 10 m width, i.e., $L_l < 10$, then herding does not occur (Heorton et al., 2017; Smedsrud & Skogseth, 2006) and the grease ice is spread in a layer of uniform thickness over the lead surface, Figure 2a. If the grease layer is thicker than the sea ice for any part of the lead, then the grease ice thickness is reduced to match the sea ice for that lead section, $H_g = H_i$. The solid fraction of the grease ice that is thereby removed from the lead thickens the sea ice in this category, and the water fraction drains to the ocean.

Where C_i is low, some grease ice may form at large distances from ice floes and is unlikely to all be herded against ice edges, or to all overflow onto ice floes (note there

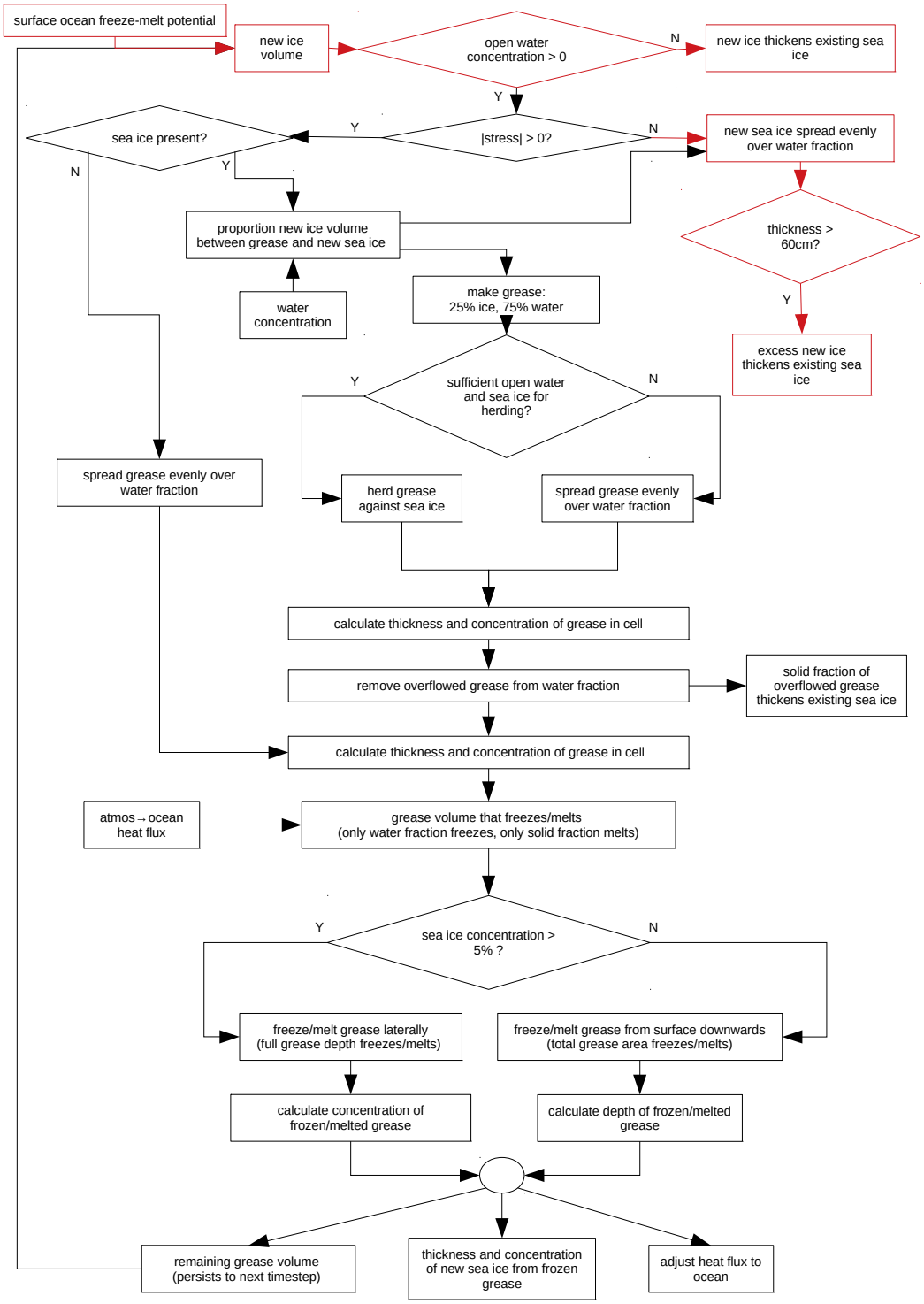

Figure 1. Outline of the new grease scheme, see text for detailed description. Steps that are unchanged from the standard scheme are outlined in red.

is no distinction in the model between under- and over-flowing). For cells with $C_i < 0.05$, any grease ice therefore forms a uniformly thick layer in the open water part of the cell.

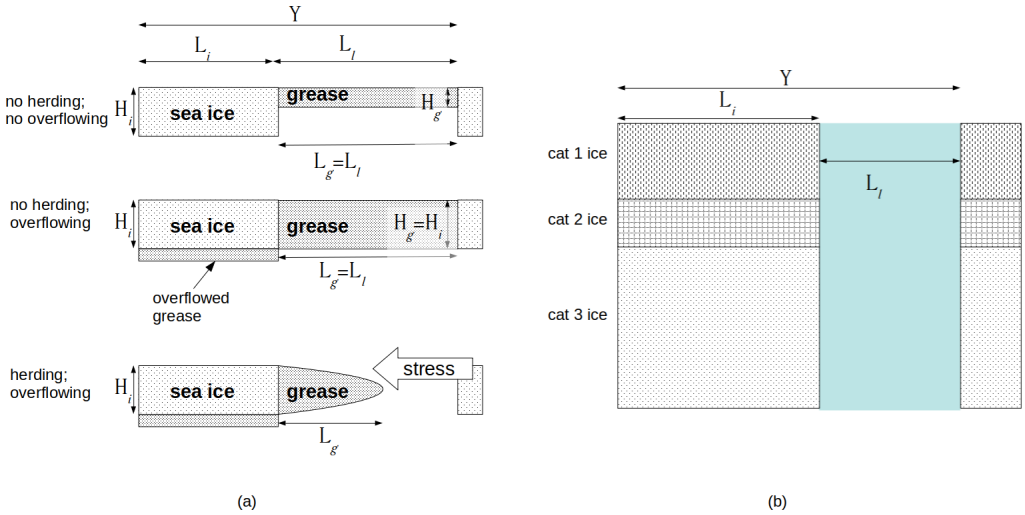

Figure 2. (a) Cross-sectional lead-sea ice element used for implementation of the grease scheme in cells with partial sea ice cover; (b) The lead-sea ice element, viewed from above.

The grease ice thickness is compared to the sea ice thickness for the different categories of existing ice, and if $H_g > H_i$, then some grease ice overflows onto the sea ice of that category. For each existing ice category, the volume of overflowed grease ice is $V_g^o = C_i(H_g - H_i)$, and the volume of grease ice in the water is updated: $V_g = V_g - V_g^o$. This treatment means that grease ice remaining in the open water may be thicker than the existing sea ice, but it is considered more realistic than piling grease ice formed over a large open water area onto small ice floes, potentially thickening them by an unrealistically high amount.

3.1.2 Herding

For cells with $C_i > 0.05$ and $L_l > 10$, grease ice may be subject to herding, i.e., may be piled up against (and overflow onto) the sea ice by atmospheric and oceanic stress, forming the wedge shape in Figure 2a rather than being distributed in a layer of even thickness (Heorton et al., 2017; Wilchinsky et al., 2015; Smedsrud & Martin, 2015; Smedsrud, 2011). We follow Wilchinsky et al. (2015) and project the stress onto the leads, somewhat arbitrarily assuming all leads to be orientated at 30°to the stress direction (HadGEM3-GC3.1 contains no information on sub-grid scale lead orientation). Using the projected stress to implement the model proposed by Smedsrud (2011), we calculate the concentration and thickness of the herded grease ice in the lead, and the volume of any grease ice that overflows onto the sea ice, V_g^o for each lead part (i.e., for each part of the lead that has walls corresponding to a specific ice thickness category, Figure 2b).

Assuming the thick end of the grease ice wedge has thickness H_i, Equation (1) determines the maximum possible span of grease ice that the lead can accommodate, L_g^{max}, from the stress, τ, and the granular resistance of the grease ice, k_r, Figure 3. Note that this is the maximum span available for the grease ice to occupy, and the actual span (calculated later) may be smaller if there is insuffcient grease ice to fill this span. The granular resistance, k_r, can be thought of as the resistance of the grease ice to a solid wall moving through it, with units Nm^{-3}. If the wall exerts force (per unit length of wall), F, over a grease ice depth, H_g, then the wall will move with constant speed, i.e., the resistive force from the grease ice will match F, if $F = k_r H_g^2$ (Smedsrud, 2011). If the

lead is not wide enough to accommodate L_g^{max} (i.e., $L_g^{max} > L_l$), then the wedge is truncated, Figure 3b. In this case, we set $L_g^{max} = L_l$, and calculate the thickness of the thin end of the wedge, H_g^{min}, from Equation (2). If the wedge is not truncated (Figure 3a), then $H_g^{min} = 0$.

$$L_g^{max} = max\left\{\frac{k_r H_i^2}{\tau}, L_l\right\} \tag{1}$$

$$H_g^{min} = \sqrt{H_i^2 - \left(L_l \frac{\tau}{k_r}\right)} \tag{2}$$

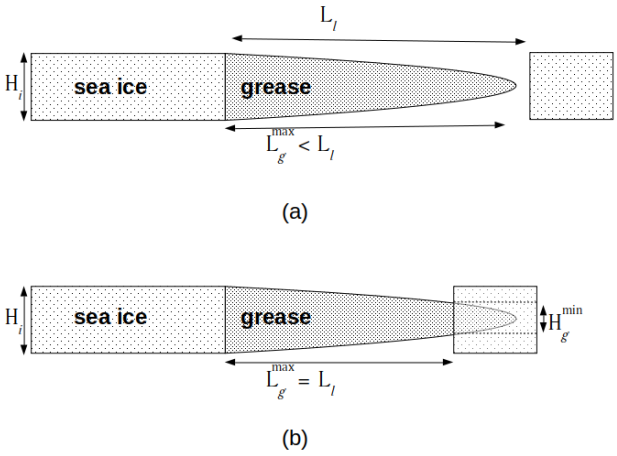

Figure 3. Cross-section of the wedge shape occupied by herded grease ice in a lead with the maximum possible grease ice span, L_g^{max}: (a) when the maximum span can be accommodated in the lead; (b) when the wedge shape is truncated so that the maximum grease ice span can be contained within the lead.

Having defined the wedge shape corresponding to the largest grease ice span allowed by τ, H_i, k_r and L_l, we follow Wilchinsky et al. (2015) and use Equation (3) to calculate the corresponding grease ice volume, V_g^{max}. This is the maximum grease ice volume that can be accommodated in the lead without overflowing.

$$V_g^{max} = \frac{2k_r}{3\tau}\left(\left(L_g^{max}\frac{\tau}{k_r} + {H_g^{min}}^2\right)^{\frac{3}{2}} - {H_g^{min}}^3\right) \tag{3}$$

If V_g^{max} is greater than the actual volume of grease ice, V_g, then all the grease ice can be accommodated in the lead and there is no overflowing. Continuing to follow Wilchinsky et al. (2015), the actual span of the grease ice, L_g, is then given by Equation (4).

$$L_g = \frac{k_r}{\tau}\left(\frac{3\tau V_g}{2k_r}\right)^{\frac{2}{3}} \tag{4}$$

If V_g^{max} is less than V_g, then the excess grease ice volume overflows onto the sea ice, $V_g^o = V_g - V_g^{max}$, and the volume of grease ice remaining in the lead is updated: $V_g = V_g^{max}$. The solid part of the overflowed grease ice thickens the existing ice, and

the water part drains to the ocean. Equations 1 - 4 are carried out separately for each lead part (lead parts are defined by different values of H_i, e.g., for the parts of the lead associated with different ice thickness categories in Figure 2b). The grease ice concentration, C_g^n, and thickness, H_g^n, are now determined for each lead part, n, from Equations (5) and (6), where V_g is now the updated grease ice volume. The total grease ice concentration is $C_g = \sum_n C_g^n$, where C_i^n is the concentration of sea ice in the thickness category corresponding to lead part n, so $C_i = \sum_n C_i^n$.

$$C_g^n = \frac{L_g C_i^n}{Y C_i} \tag{5}$$

$$H_g^n = \frac{V_g}{L_g} \tag{6}$$

3.2 New Sea Ice

Once grease ice concentration and thickness have been calculated, the atmosphere to ocean heat flux, $Q_{a\to o}$, determines whether any, or all, of the grease ice melts back into the ocean, freezes to become new sea ice (depending on the sign of $Q_{a\to o}$), or persists as grease ice to the next model timestep.

The latent heat of freezing is used to calculate the volume of water that can be frozen by $Q_{a\to o}$ (or the volume of ice that can be melted). This is converted to the equivalent grease ice volume, accounting for the fact that only the water fraction of the grease ice can freeze, and only the solid fraction can melt.

The concentration and thickness of any new sea ice is then determined from the concentration and thickness of grease ice, and by the magnitude of $Q_{a\to o}$, following Wilchinsky et al. (2015). The latent heat associated with this freeze (or melt) is added to (or subtracted from) the ice to ocean heat flux that is returned from the sea ice model to the ocean model . For cells with low ice concentration ($C_i < 0.05$), any freezing or melting occurs from the surface downwards, i.e., the surface of the grease ice layer freezes (or melts) first, and the volume of grease ice to be frozen (or melted) determines the depth to which freezing (or melting) occurs. The concentration of the new sea ice is then the grease ice concentration, C_g, and the thickness of the new sea ice is the depth to which the grease ice froze. Conversely, for cells with $C_i > 0.05$, we assume that the grease ice occupies leads in the sea ice, and freezing and melting occur laterally at the lead walls, i.e., the full depth of the grease ice layer freezes (or melts), and the volume of grease ice to be frozen (or melted) determines the concentration of grease ice that freezes (or melts). In this case, the thickness of the new sea ice is the thickness of the grease ice, and the concentration is the concentration of the grease ice that froze. The grease ice volume is reduced by the volume of grease ice that has melted or frozen into new sea ice. If not all of the grease ice has frozen or melted, then the remainder persists to the next model timestep where the solid fraction is added to the volume of new ice created from the surface ocean freeze-melt potential, Figure 1.

3.3 Transport

When sea ice in a cell is transported in the dynamics part of the sea ice model, any grease ice that remains in the cell after the freeze-melt steps above is transported with it as a passive tracer (grease ice only exists in the sea ice component of the model, not the ocean component). To avoid grease ice in ice-free cells remaining static, cells containing grease ice are required to have $C_i > 0.00005$ in at least one sea ice category (in the standard HadGEM3-GC3.1 configuration of GSI8.1, sea ice is removed from categories with concentration lower than this prior to transport). For cells where the sea ice concentration is too low, any sea ice volume in the thinnest sea ice category (which may

be up to 60 cm thick), is 'spread out' over the cell in an attempt to achieve $C_i > 0.00005$. If this does not result in a layer of sea ice that is at least 20 cm thick, then the solid fraction of some of the grease ice is considered to be new sea ice and removed from the persisting grease ice volume. If there is insufficient grease ice to create 20 cm thick layer with $C_i > 0.00005$, then all the grease ice is used and thinner sea ice is created. This has the effect of facilitating transport of the remaining grease ice (note that in standard HadGEM3-GC3.1 model simulations, the solid fraction of the whole grease ice volume would be considered new sea ice).

3.4 Caveats to the Grease Scheme

This first attempt to represent grease ice in a fully coupled climate model makes the model more physically representative. More comprehensive observations of grease ice properties would allow some necessary simplifications to be addressed. For example, grease ice in our model does not alter the surface roughness or radiative properties of the ocean surface, despite these being different for water- and grease ice-covered surfaces.

We assume a fixed solid fraction of 25% for grease ice, which is within the range of reported values observed in-situ and in laboratory experiments (Maus & De La Rosa, 2012; Smedsrud & Skogseth, 2006; Winsor & Björk, 2000; Martin & Kauffman, 1981). In reality, however, the solid fraction is likely to increase as grease ice solidifies into sea ice, as observed in Smedsrud and Skogseth (2006) and described by Maus and De La Rosa (2012), however more observations are needed to define or parameterise a globally realistic rate for the increase. In our implementation of the grease scheme, brine rejection is only associated with the formation of new sea ice, and there is no change to ocean salinity when grease ice forms or melts. In reality, the gradual release of brine as grease ice solidifies into sea ice can result in a more gradual salinification of ocean surface waters (Skogseth et al., 2009), which may have implications for local hydrography in some places (Smedsrud & Skogseth, 2006). It is also likely that the water content of grease ice is more saline than the ambient ocean water (Heorton et al., 2017; Smedsrud & Skogseth, 2006), and should therefore be associated with a lower freezing temperature. A range of salinities have been observed for grease ice, e.g., Smedsrud and Skogseth (2006), making it difficult to define an appropriate deviation from the ambient salinity. We therefore neglect this and assume the salinity-dependant freezing temperature of water in grease ice to be that for the ambient ocean water. This means that the freezing of water within the grease ice may be associated with a slightly smaller energy change than is realistic.

Where grease ice forms in partially ice-covered cells and is subject to herding, a value for its granular resistance is required (k_r in Equation (1)). This is a function of the internal friction angle (Lambe & Whitman, 1979), and the grease ice bulk porosity (Dai et al., 2004), which are not well known. We set $k_r = 866$ Nm^{-3}, following Wilchinsky et al. (2015). Sensitivity tests in that study showed that higher values of k_r result in less herding, which may mean that leads freeze over faster and newly formed sea ice is thinner. A similar sensitivity was shown for the assumed lead orientation: smaller angles relative to the stress direction result in less herding since the drag stress perpendicular to the lead is reduced (Wilchinsky et al., 2015). However, the value for this orientation angle is necessarily arbitrary since the model contains no information on the orientation of sub-grid scale leads. The width of the lead-sea ice element, Y, in Figure 2 is set at 5 km, following Wilchinsky et al. (2015), however Heorton et al. (2017) show the degree to which grease ice is herded against the lead walls is sensitive to this, and Smedsrud and Martin (2015) suggest that the square root of the grid cell area may be more appropriate. At high latitudes, this would mean a different value for different cells, with particularly large differences at the latitudes where sea ice advances and retreats each year. Setting this value too low, or assuming an inappropriately low angle for the lead orientation has an effect equivalent to that which results from setting k_r too high (Wilchinsky et al., 2015), i.e., less herding may result than is realistic.

4 Impact of Implementing the Grease Scheme

Changes were made to the ocean and sea ice components of HadGEM3-GC3.1 to implement the new scheme for global coupled land-ocean-sea ice-atmosphere simulations. We performed a three member ensemble using historical forcings from 1964 to 2014 to account for internal variability. There was no discernible impact on computation time. Data from these simulations are referred to as GREASE. Using historical forcings allows any impact of the scheme to be assessed in the context of data derived from observations. Sea ice area and thickness have a high degree of natural variability, and we therefore use a three member ensemble of simulations with grease ice included, for comparison against an equivalent ensemble using the standard sea ice formation scheme. Three of the historical simulations submitted to CMIP6 (Eyring et al., 2016) by the UK Met Office comprise our control, and data from these are referred to as STANDARD. Note that the ensemble members all use the same historical forcings, but are branched from the pre-industrial control simulation (Menary et al., 2018) at points in that simulation when the ocean is in different states. To provide context for the difference between the sea ice area in STANDARD and GREASE, we show total sea ice area derived from satellite-bourne observations using two different algorithms: bootstrapping (Comiso, 2017) and the NASA Team algorithm (Cavalieri et al., 1996), referred to as BOOTSTRAP and NASATEAM respectively. To assess any impact of the grease scheme on sea ice thickness and volume, we use data from the Pan-Arctic Ice Ocean Modeling and Assimilation System (PIOMAS) for the Arctic, which combines satellite-derived sea ice concentration and sea surface temperatures with modelling (Schweiger et al., 2011), and for the Antarctic, we use data from the Global Ice-Ocean Modeling and Assimilation System (GIOMAS), which combines satellite-derived sea ice concentration with modeling (Zhang & Rothrock, 2003). PIOMAS data agree well with some sea ice thickness observations in the Arctic (Stroeve et al., 2014), but a comparison study of different thickness datasets derived from remote observations, including PIOMAS, found all derived sea ice thickness data to be associated with reasonably high uncertainty (Wang et al., 2016). In particular, PIOMAS may underestimate the thickness of thick ice and underestimate the thickness of thin ice (Wang et al., 2016). A paucity of observations means that GIOMAS data have not been validated in the Antarctic to our knowledge, although they have been shown to agree reasonably well with observations in the Arctic (Zhang & Rothrock, 2003). Nonetheless, in the absence of spatially comprehensive Antarctic observations, GIOMAS provides a useful dataset, derived partially from observations, for comparison with model results (and has been used as such in other studies, e.g., (Shu et al., 2015)).

The period of overlap for the model and observation-derived datasets is 1979 - 2013 and the mean annual cycle in total sea ice area over this period is shown for all datasets in Figure 4. Implementing the grease scheme does not affect the timing or magnitude of the seasonal cycle in total sea ice area (timeseries of sea ice area for the months corresponding to the maximum and minimum are shown in Figure A1). In the Arctic, the maximum and minimum occur in March and August respectively, in agreement with the observation-derived data. In the Antarctic, the maximum and minimum occur in September and February respectively, making the maximum a month later in GREASE and STANDARD than in the observation-derived data. The distribution of sea ice thicknesses for these months from GREASE and STANDARD over the period 1979 to 2013 is shown in Figure 5, alongside the distributions in PIOMAS and GIOMAS thickness for the same period.

The spatial distribution of effects from the grease scheme is discussed with reference to the geographical areas marked in Figure 7. The maps in Figures 8 to 11 show the spatial distribution of the average sea ice concentration and thickness for GREASE and STANDARD, and the difference between them, for 1979 - 2013. Sea ice concentration from the monthly climatology derived from NASATEAM data for 1979 - 2018 (Stroeve

et al., 2014), and thickness maps from PIOMAS and GIOMAS data over 1979 - 2013 are also shown for context.

To assess changes to the processes driving sea ice formation, Figures 12 and 13 show the mean rate of change in sea ice concentration attributable to thermodynamic and dynamic processes respectively, for November and June, which Figure 4 shows to be midway through the sea ice growth period for the Arctic and Antarctic respectively. The ocean mixed layer depth, defined using a threshold of a 0.01 kgm^{-3} change in density with respect to the density at 10 m depth, is also shown for June and November, Figure 14.

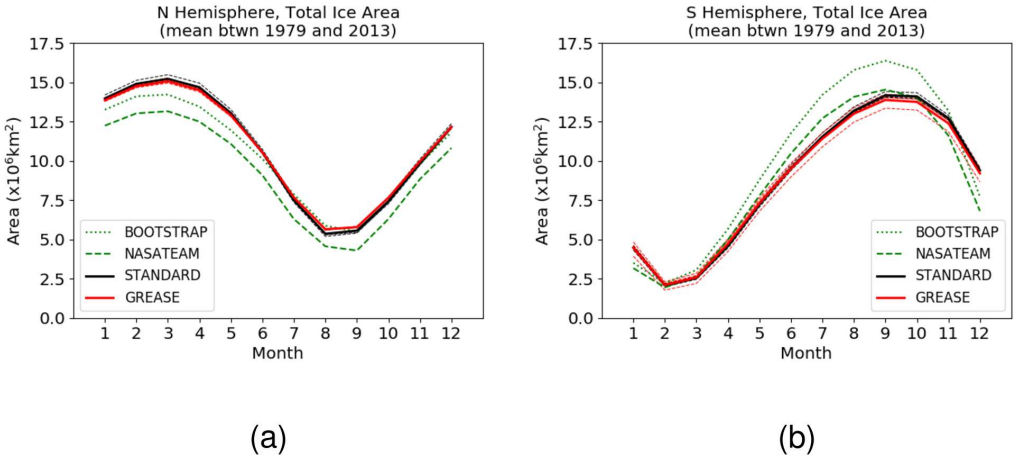

Figure 4. Mean seasonal cycle for total sea ice area 1979 to 2013. Bold red and black lines are ensemble means for GREASE and STANDARD, dashed lines in the same colors are individual ensemble members. (a) Arctic; (b) Antarctic.

5 Impacts in the Arctic

In the Arctic, GREASE and STANDARD capture the sea ice minimum area well according to BOOTSTRAP, but overestimate the magnitude of the winter maximum area according to both BOOTSTRAP and NASATEAM, Figure 4a. In this work we restrict ourselves to a discussion of the impact of the grease scheme, using the observation-derived datasets for context, rather than discussing differences between the model and observation-derived data more widely.

The range of Arctic ice thicknesses simulated in GREASE is broader than in STANDARD, and includes thicker ice in both summer and winter, Figure 5a, b. Herding of grease ice against the sea ice edge, and the lateral growth of new sea ice forming in leads, means that new sea ice in GREASE may be thicker than new sea ice forming in STANDARD. In GREASE, new sea ice forming in a partially ice-covered cell may be as thick as the existing sea ice, whereas in STANDARD, new sea ice has a uniform thickness of up to 60 cm, which is exceeded only once the grid cell has become completely ice covered. The PIOMAS thickness distributions in Figure 5a and b do not have the bimodal shape of the STANDARD and GREASE distributions. The two modes represent single- and multi- year ice, and the latter is broadened when the grease scheme is implemented because grease ice herded in leads against the edge of thick multiyear sea ice persists and consolidates into new sea ice with a thickness that may match the multiyear sea ice thickness. The single mode in PIOMAS may reflect an underestimation of thick ice thicknesses

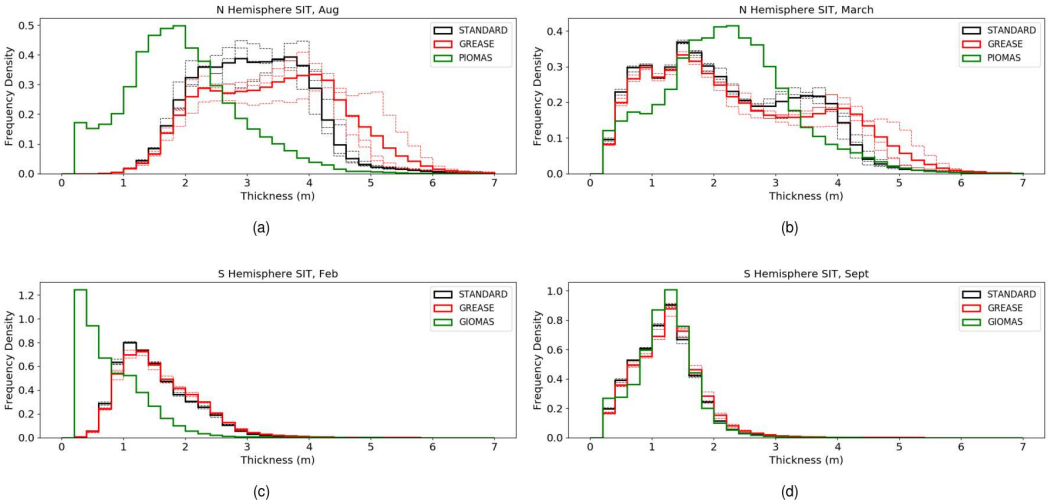

Figure 5. Normalised distribution of all sea ice thicknesses (weighted by ice area) in each dataset for 1979 to 2013. Ensemble means are in bold, dashed lines are individual ensemble members. The distribution is normalised such that the integral is one (i.e, Σ_{bins}[bin width times frequency density for that bin]=1). The bin width corresponds to a 20 cm thickness range. (a) August, Arctic; (b) March, Arctic; (c) February, Antarctic; (d) September, Antarctic. Note the different scales.

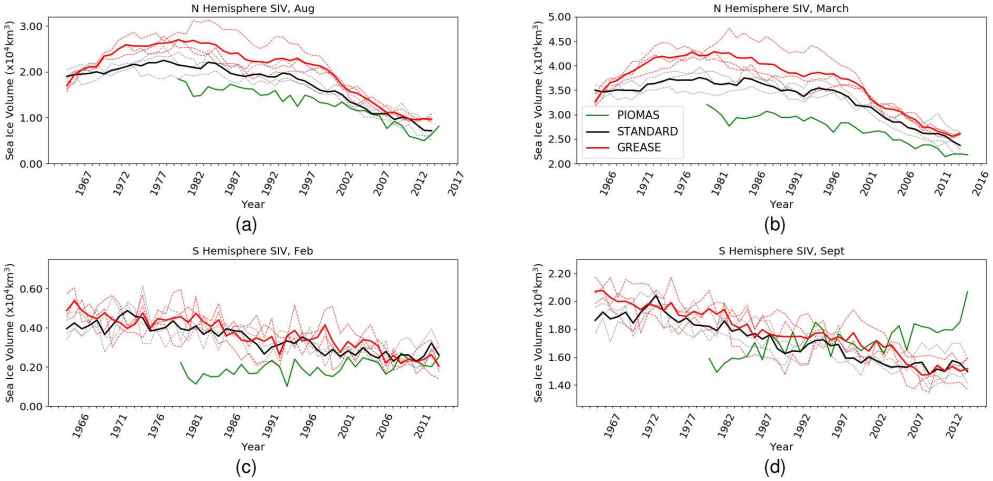

Figure 6. Total sea ice volume. Ensemble means for GREASE and STANDARD are in bold, dashed lines are individual ensemble members. (a) August, Arctic; (b) March, Arctic; (c) February, Antarctic; (d) September, Antarctic. Note the different scales.

in PIOMAS in summer and winter, combined with an overestimation of thin ice thicknesses in winter, as suggested in Wang et al. (2016). There is known to be a cold bias in the standard HadGEM3-GC3.1 historical simulations that leads to an overestimation of Arctic sea ice thickness (Kuhlbrodt et al., 2018). There is therefore likely to be too much thick Arctic sea ice in STANDARD, and this bias increases in GREASE, when the grease ice scheme is implemented.

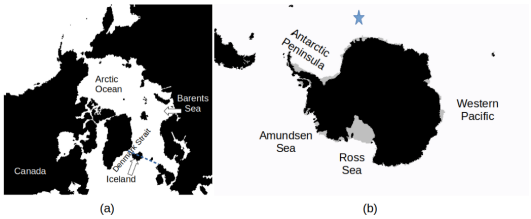

Figure 7. The maps show areas referred to in the discussion of local effects of the grease scheme. (a) Arctic (the dashed line illustrates the approximate location of the Greenland-Scotland Ridge); (b) Antarctic (the star illustrates the approximate location of the Weddell Sea Polynya).

The total Arctic sea ice volume is greater in GREASE than in STANDARD for most of the simulated period, Figure 6a, b. In conditions of non-negligible oceanic and/or wind stress, the grease scheme introduces a delay to the formation of new sea ice, as grease ice is first created, and new sea ice may not form until timestep(s) after the surface becomes supercooled (in contrast to STANDARD, where surface supercooling is transformed instantly to new sea ice). Also, new sea ice formed from frozen grease ice is thicker than the nilas that is formed in STANDARD, as discussed above, and is less likely to cover the open water fraction of a grid cell. Areas of open water therefore take longer to freeze over in GREASE than in STANDARD, leaving the ocean subject to increased atmospheric cooling and driving the production of an increased volume of sea ice in GREASE, relative to STANDARD. The total Arctic sea ice volume simulated in GREASE and STANDARD becomes more similar towards the end of the timeseries, reflecting the warming of the ocean and atmosphere in recent decades (a warmer ocean requires a greater degree of cooling in order to freeze, and the cooling provided by the atmosphere is reduced as the atmosphere warms).

There are some small local differences in sea ice concentration between GREASE and STANDARD in Figure 8, with the grease scheme giving a slight decrease in some areas in winter and a slight increase in summer. The winter decrease occurs at locations where the STANDARD concentration is higher than the NASATEAM climatology, and so brings the model slightly closer to the observation-derived data. The summer concentration increases in GREASE, however, occur mainly at the edge of the summer ice pack, where concentration in STANDARD is already higher than in the climatology. Implementing the grease scheme therefore pushes the summer concentration in the model further from the climatology, however figure 4 shows the NASATEAM algorithm, from which the climatology is derived, underestimates ice area relative to the bootstrap algorithm, and the climatology may therefore show too small an ice-covered area.

The effect on Arctic sea ice thickness is much greater than the effect on concentration, and ice simulated in GREASE is thicker than in STANDARD for most of the Arctic Ocean in both winter and summer, Figure 9. An exception to this is the northern Barents Sea, where the winter ice is slightly thinner in GREASE than in STANDARD. The thickening in GREASE enhances what is already a positive thickness bias in STANDARD, relative to PIOMAS. This could be attributable to the assumptions made in the grease scheme that determine the degree to which the grease ice is herded against lead edges, or may be attributable to partially compensating biases elsewhere in the model. Alternatively, Arctic sea ice thickness may be underestimated in the PIOMAS data, as suggested by the single mode in the thickness distribution in figure 5a, b, which does not differentiate between single- and multiyear ice.

In both GREASE and STANDARD, new sea ice forms thermodynamically in the Arctic Ocean and along coastlines in the Arctic, Figures 12a, c. It is transported to the edges of the Arctic Ocean to where it melts, this can be seen in 13a, c, where negative values indicate ice divergence (i.e., ice leaving a grid cell), and positive areas show either ice moving into a grid cell or convergence of floes within a grid cell (reducing the total concentration in the cell). The effect of the grease scheme on these processes in the Arctic is very small, and is mostly confined to the edges of the sea ice pack. This is not surprising since Figures 12 and 13 reflect changes in sea ice concentration, which Figure 8 shows to be only slightly affected by the grease scheme in the Arctic.

The widespread thickness changes in response to the grease scheme are greater than may be expected from the increased cooling that follows from the increased open water area, since Figure 8, f shows only a slight increase in open water area. It is, however, possible that leads remain open for longer in GREASE, leading to production of an increased ice volume as discussed above, but that when they freeze over the ice that fills them is thicker, and less likely to fracture again and create a new lead. The sea ice concentration may therefore remain largely unchanged, but in GREASE the leads may persist for longer and occur less frequently. A smaller number of longer-lived leads may result in more ocean cooling than a greater number of short-lived leads, despite the open water area remaining equivalent, if the longer opening time allows convection to develop in the underlying near-surface ocean layers. As the exposed ocean surface cools, the cooled (and therefore denser) water sinks, driving an upwelling of warmer water from below, which then cools and sinks, creating an overturning cell. The upwelling of warmer waters allows the ocean to lose more heat to the atmosphere, and so there is a greater cooling effect than occurs if just the exposed surface water layer cools and freezes. The increased cooling drives increased frazil production, and therefore increased sea ice production. This effect can occur even for relatively shallow convection depths. Figure 14e shows some deepening of the winter mixed layer under the pack ice in the central Arctic Ocean in GREASE, relative to STANDARD, which suggests increased convection and so supports this theory (note that the strong deepening of the mixed layer in the Barents Sea is not statistically significant). There is a shallowing of the winter mixed layer to the south of Iceland in GREASE, indicating increased stratification driven by the higher volumes of melt water exported out of the Arctic through the Denmark Strait in GREASE, following the greater volume of sea ice in GREASE, relative to STANDARD. There is also a deepening of the winter mixed layer on the north-eastern side of the Greenland-Scotland ridge, and a shallowing on the south-western side, in GREASE, relative to STANDARD in Figure 14e. Atmospheric cooling creates dense water that sinks on the north-eastern side of the ridge, and then flows south, rising to cross the ridge before sinking below lighter, warmer water carried northwards by The North Atlantic Current. Increases in convection on the north side of the ridge, and in stratification on the south side, may indicate increased atmospheric cooling of surface waters on the north side of the ridge but this is an area where the mixed layer is already reasonably deep in STANDARD, making the anomaly relatively small. It is difficult to attribute this effect to changes in the model sea ice formation processes, but further investigation, although beyond the scope of this manuscript, may be worthwhile.

6 Impacts in the Antarctic

Both GREASE and STANDARD underestimate the maximum Antarctic sea ice area, relative to BOOTSTRAP, but agree well with NASATEAM, although as noted earlier the simulated maximum occurs around a month later in GREASE and STANDARD. The trend in simulated maximum Antarctic sea ice area is largely unaffected by the implementation of the grease scheme, and both GREASE and STANDARD overestimate the rate of decline relative to BOOTSTRAP and NASATEAM, Figures A1c, d.The distributions of sea ice thicknesses in GREASE and STANDARD are similar for both sum-

mer and winter, but include thicker ice than GIOMAS in summer, Figure 5c, d. The decreasing trend in summer and winter sea ice volume is also unaffected by the implementation of the grease scheme, and disagrees with the slightly increasing trend in both of these fields in GIOMAS, Figure 6c, d.

Although there is little overall impact on total Antarctic sea ice area, volume or the overall distribution of sea ice thicknesses, Figures 4b, 5c, d, 6c, d there are large local differences in Antarctic sea ice concentration and thickness between GREASE and STANDARD, particularly in winter, Figures 10, 11.

In summer, differences in sea ice concentration between GREASE and STANDARD are small, but sea ice around the Antarctic coast is generally thicker in GREASE, Figure 11e, as open water at the coast remains open for longer, exposed to increased atmospheric cooling which drives increased sea ice production. In winter, sea ice concentration in the Amundsen Sea is much lower in GREASE than in STANDARD, and is similarly decreased (although more weakly) everywhere around the northern sea ice edge, except in the Western Pacific, where the sea ice concentration is much higher in GREASE than in STANDARD, Figure 10f. There are also changes to winter sea ice thickness, with a large increase in the Western Pacific and around the Antarctic Peninsula, a decrease in the Amundsen Sea, and some smaller areas of decrease, for example at the location associated with the Weddell Sea polynya, Figure 11. Differences in thickness are generally weaker than in the Arctic because Antarctic sea ice is thinner, and so the maximum thickness for new sea ice in GREASE is also thinner, making it closer to the maximum thickness allowed in STANDARD (note that the scale in Figure 9b, c is different to that in Figure 11b, c).

Around the Antarctic coast in both GREASE and STANDARD, sea ice concentration increases thermodynamically in coastal polynyas, Figure 12b, d, and is transported offshore, as shown by the areas of sea ice divergence in Figure 13b, d (coastal polynyas can be identified as areas of low concentration and thickness next to the coast in Figures 10a, b and 11a,b). In GREASE, the production of grease ice in place of at least some of the sea ice that forms instantly in the polynyas in STANDARD, means that these areas of open water are likely to remain exposed to atmospheric cooling for longer. This increased cooling drives an increase in sea ice production. Because the grease ice does not freeze instantly and is subject to transport (grease ice is transported by the same wind and ocean stresses that drive sea ice divergence in Figure 13b, d), there may be a decrease in sea ice formation at the coast, and an increase slightly north of the coast, where the transported grease ice freezes. This effect can be seen in the Western Pacific, where sea ice production at the coast is reduced in GREASE (relative to STANDARD) because grease ice is produced instead of sea ice, creating a negative anomaly in Figure 12f. Sea ice divergence at the Western Pacific coast then also reduces, since grease ice is transported instead of sea ice, creating a positive anomaly in Figure 13f. North of these coastal anomalies, thermodynamic sea ice production increases in GREASE as the transported grease ice freezes to form new sea ice, Figure 12f. The increase in sea ice concentration and thickness in the Western Pacific in GREASE, relative to STANDARD, (Figures 10f and 11f) therefore follows from the enhanced surface cooling at the coastal polynyas, despite the increase being slightly displaced from the coast. The increased volume of sea ice forming in this area leads to an increase in the sea ice divergence that transports ice to the northern sea ice edge in the Western Pacific, Figure 13f. This leads to an increase in melt (note that Figure 12 only includes changes in ice concentration, and so the melting of equal areas of thick and thin ice appear the same), which drives an increase in ocean stratification, shallowing the surface mixed layer in the Western Pacific in Figure 14f in GREASE.

Similar processes explain the reduction in sea ice concentration and thickness in the Amundsen Sea in GREASE, relative to STANDARD, Figures 10f and 11f. There is a decrease in thermodynamic sea ice production towards the northern ice edge here in

GREASE, relative to STANDARD, where the surface mixed layer depth is high in both STANDARD and GREASE, Figure 14b, d, indicating that some convection occurs. In areas of convection, warmer water rises to the surface where it cools and sinks, driving a convective overturning and often maintaining an area of open water within the sea ice cover (a polynya). The supercooled surface water is transformed to sea ice in STANDARD, but in GREASE, the supercooling drives production of grease ice in place of at least some of the sea ice, creating the negative anomaly close to (but south of) the Amundsen Sea northern ice edge in Figure 12f. In STANDARD, sea ice divergence transports the ice from here to the northern ice edge where it melts. In GREASE, at least some of the grease ice is transported to the ice edge where it melts, without ever having frozen to form sea ice. This production, transport and melt of grease ice, rather than sea ice, creates the negative-positive anomaly pairs close to the northern ice edge in the Amundsen Sea in Figures 12f and 13f. The former shows a decrease in the production and melt of sea ice in GREASE, since grease ice is produced and melts instead, and the latter shows a reduction in sea ice divergence to the northern ice edge in GREASE, since grease ice is transported instead.

The production of grease ice in place of at least some of the sea ice that forms in STANDARD, means that open water areas freeze over less readily in GREASE, enhancing atmospheric surface cooling and driving increased convection. This results in a deepening of the mixed layer in the Amundsen Sea in GREASE (relative to STANDARD), Figure 14f. Ordinarily, increased surface supercooling is associated with increased sea ice production. However, the proximity of this area to the northern ice edge means that if grease ice is produced instead of sea ice, then at least some of it is transported to the northern ice edge where it melts without ever having formed sea ice. This reduces the sea ice concentration and thickness in the outer Amundsen Sea in GREASE, relative to STANDARD, in Figures 10 and 11. This reduction is roughly equal in magnitude to the increase in the Western Pacific following the implementation of the grease scheme, and we therefore do not see the same increase in total sea ice volume in the Antarctic that we see in the Arctic.

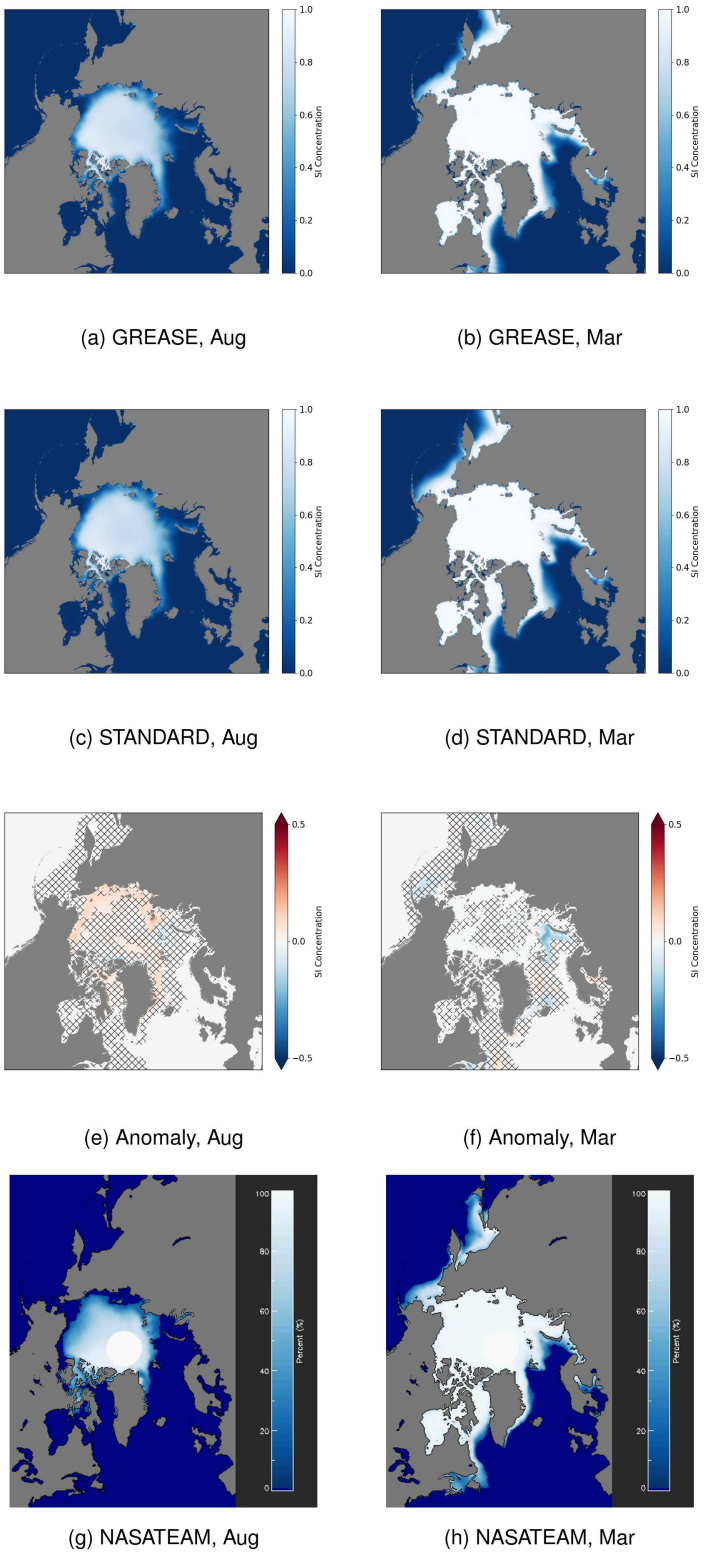

Figure 8. Arctic sea ice concentration. Ensemble mean, 1979 to 2013. Left: August; Right: March. (a) GREASE, August; (b) GREASE, March; (c) STANDARD, August; (d) STANDARD, March; (e) GREASE - STANDARD, August; (f) GREASE - STANDARD, March; (g) NASATEAM climatology, August 1979-2018; (h) NASATEAM climatology, March 1979-2018. Hatching marks areas not significant at the 95% confidence level following a student t-test. Note the polar hole in the satellite-derived climatology, indicating no data.

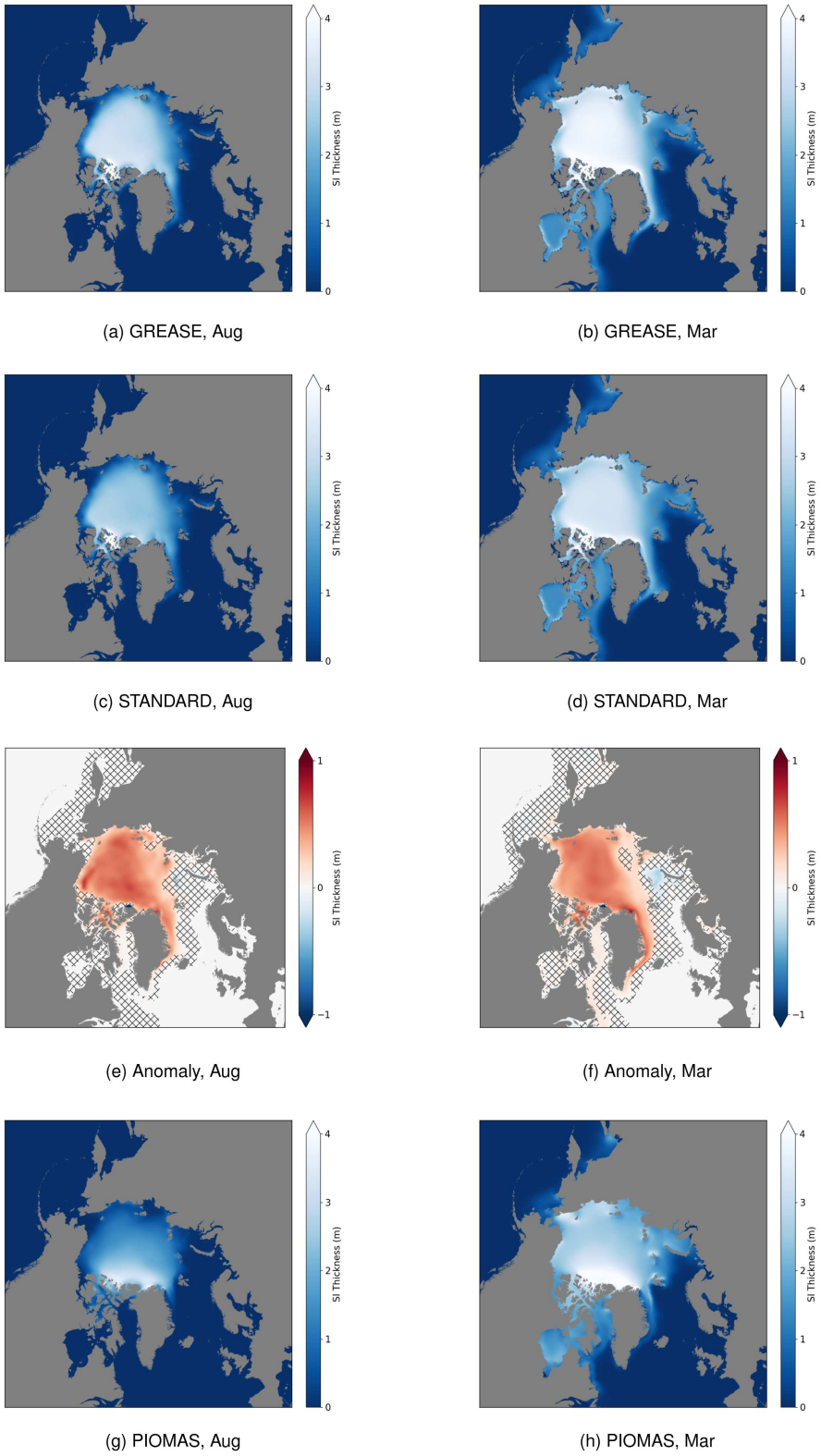

(a) GREASE, Aug (b) GREASE, Mar

(c) STANDARD, Aug (d) STANDARD, Mar

(e) Anomaly, Aug (f) Anomaly, Mar

(g) PIOMAS, Aug (h) PIOMAS, Mar

Figure 9. Arctic sea ice thickness. Ensemble mean, 1979 to 2013. Left: August; Right: March. (a) GREASE, August; (b) GREASE, March; (c) STANDARD, August; (d) STANDARD, March; (e) GREASE - STANDARD, August; (f) GREASE - STANDARD, March; (g) PIOMAS, August; (h) PIOMAS, March.

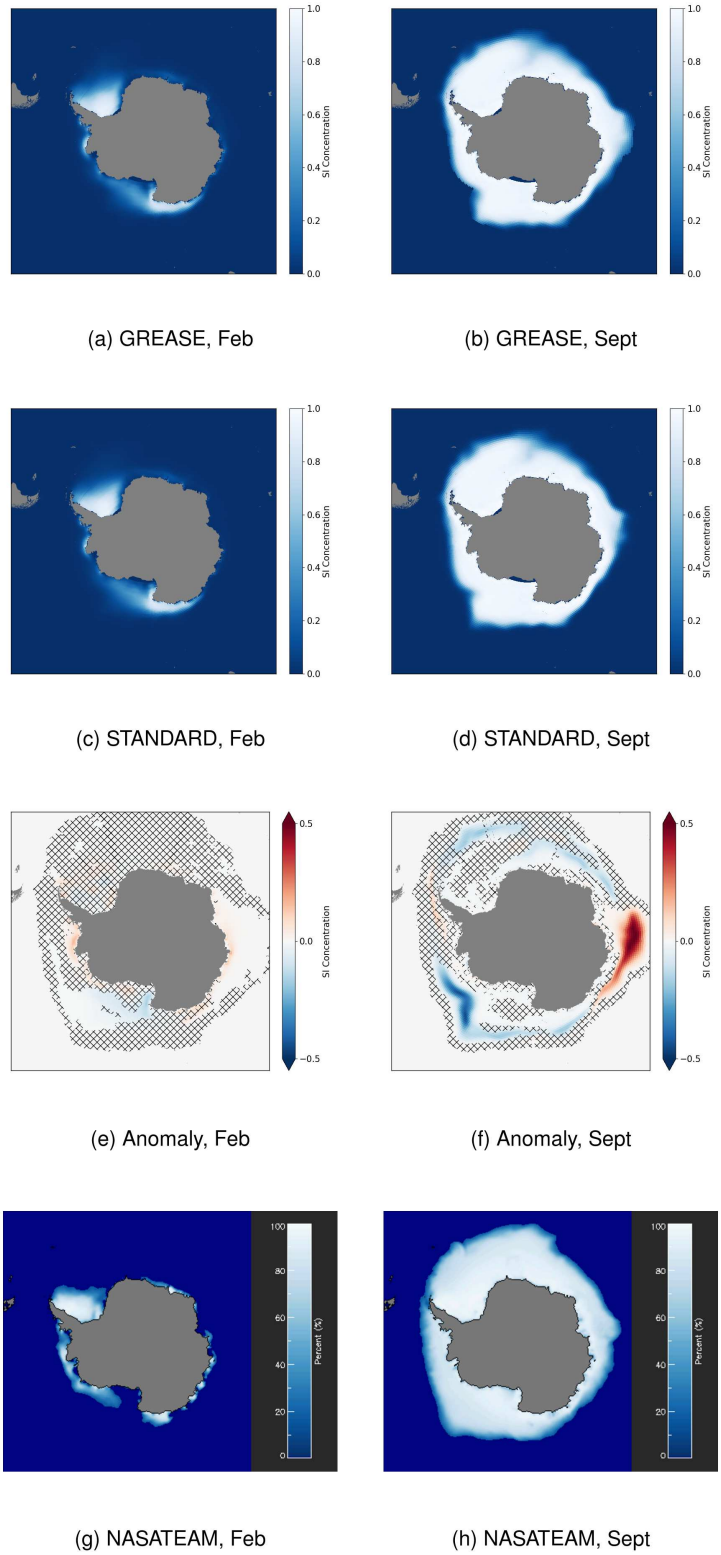

Figure 10. Antarctic sea ice concentration. Ensemble mean, 1979 to 2013. Left: February; Right: September. (a) GREASE, February; (b) GREASE, September; (c) STANDARD, February; (d) STANDARD, September; (e) GREASE - STANDARD, February; (f) GREASE - STANDARD, September; (g) NASATEAM climatology, February 1979-2018; (h) NASATEAM climatology, September 1979-2018. Hatching marks areas not significant at the 95% confidence level following a student t-test.

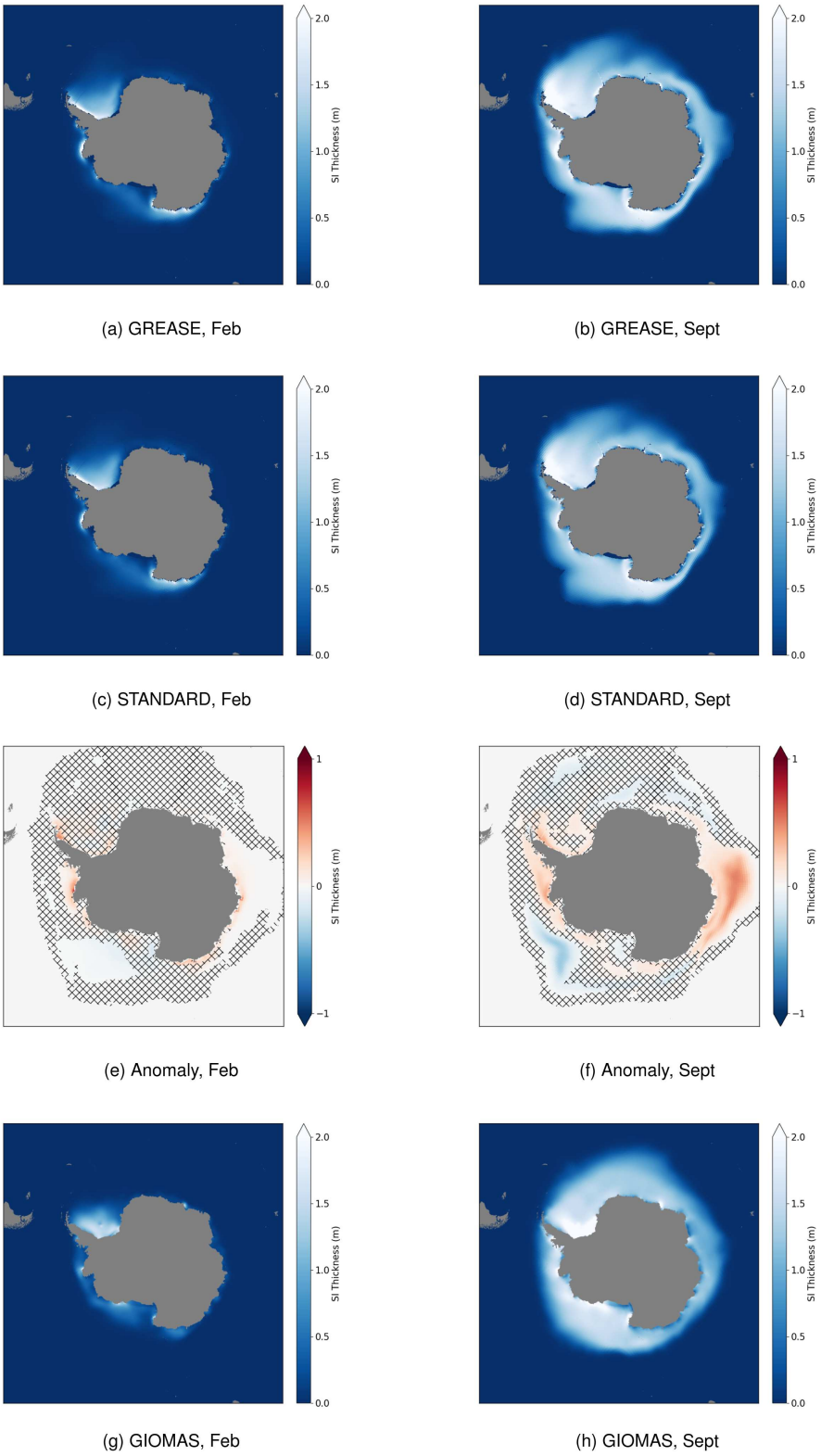

(a) GREASE, Feb (b) GREASE, Sept

(c) STANDARD, Feb (d) STANDARD, Sept

(e) Anomaly, Feb (f) Anomaly, Sept

(g) GIOMAS, Feb (h) GIOMAS, Sept

Figure 11. Antarctic sea ice thickness. Ensemble mean, 1979 to 2013. Left: February; Right: September. (a) GREASE, February; (b) GREASE, September; (c) STANDARD, February; (d) STANDARD, September; (e) GREASE - STANDARD, February; (f) GREASE - STANDARD, September; (g) GIOMAS, February; (h) GIOMAS, September. Hatching marks areas not significant at the 95% confidence level following a student t-test.

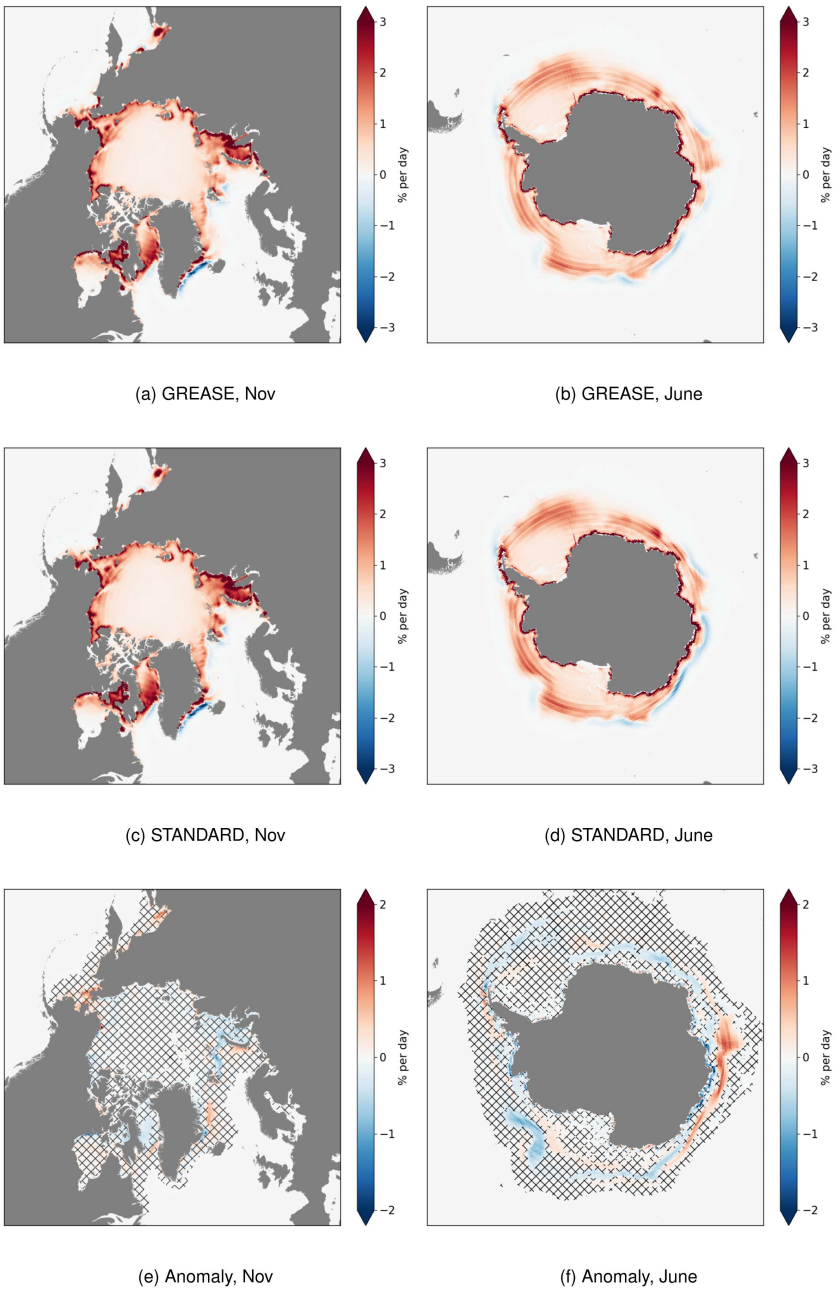

Figure 12. Change in sea ice concentration attributable to thermodynamic processes. Ensemble mean, 1964 to 2013. (a) GREASE, November; (b) GREASE, June; (c) STANDARD, November, (d) STANDARD, June; (e) GREASE - STANDARD, November; (f) GREASE - STANDARD, June. Hatching marks areas not significant at the 95% confidence level following a student t-test. Note that only sea ice is included here, not grease ice.

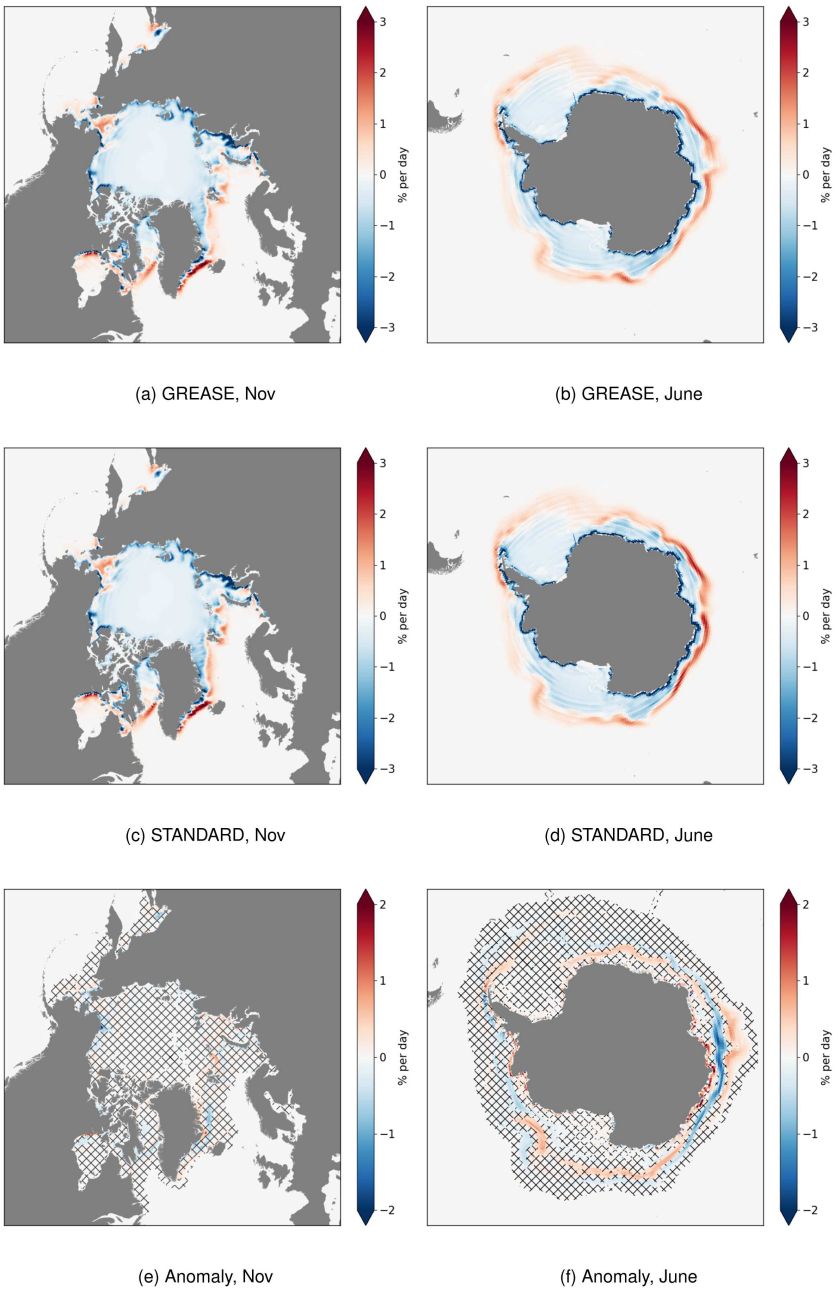

Figure 13. Change in sea ice concentration attributable to dynamic processes. Ensemble mean, 1964 to 2013. (a) GREASE, November; (b) GREASE, June; (c) STANDARD, November, (d) STANDARD, June; (e) GREASE - STANDARD, November; (f) GREASE - STANDARD, June. Hatching marks areas not significant at the 95% confidence level following a student t-test. Note that only sea ice is included here, not grease ice.

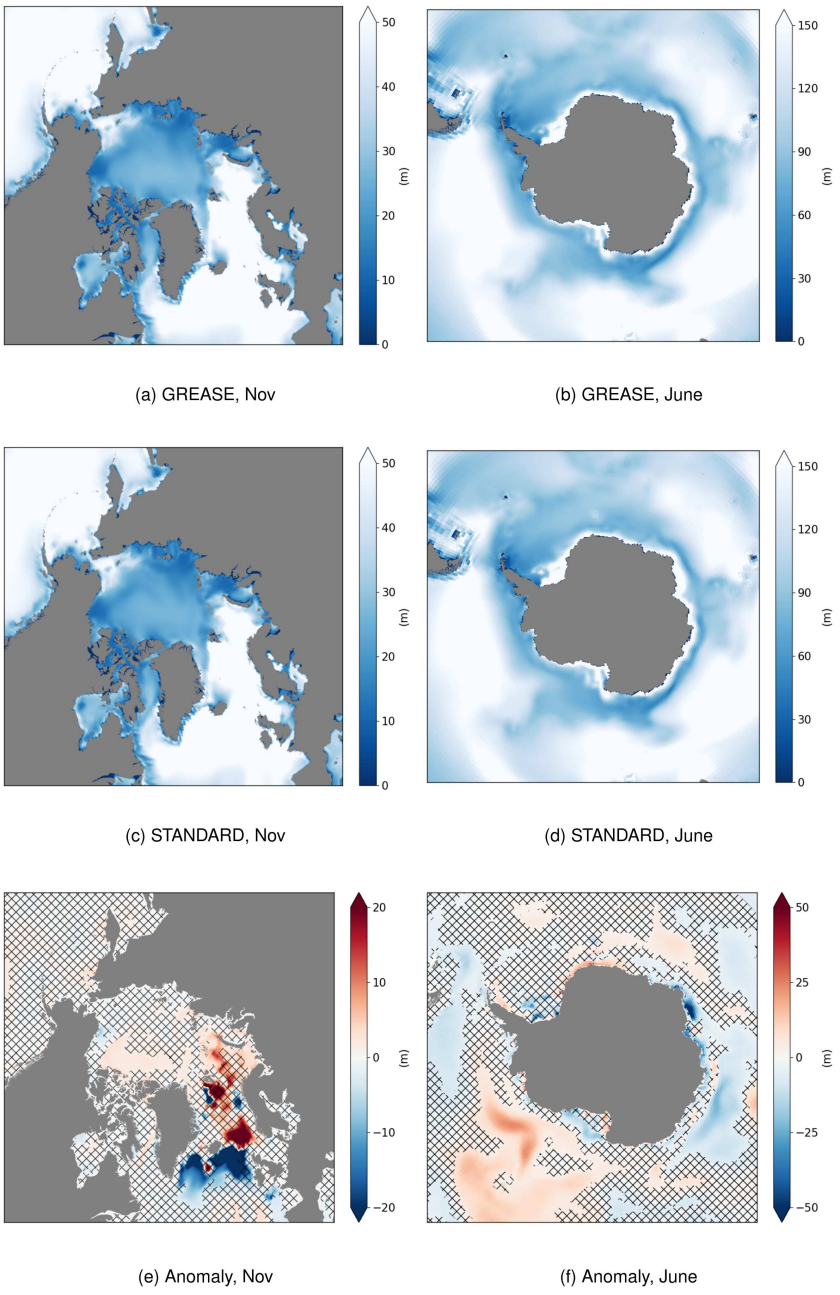

Figure 14. Ocean mixed layer depth. (a) GREASE, November; (b) GREASE, June; (c) STANDARD, November, (d) STANDARD, June; (e) GREASE - STANDARD, November; (f) GREASE - STANDARD, June. Note the different scales for the Arctic and Antarctic. Hatching marks areas not significant at the 95% confidence level following a student t-test.

7 Summary and Concluding Remarks

We have demonstrated a framework whereby grease ice formation and grease ice herding processes can be represented in sea ice formation calculations in a fully coupled global climate model. Whereas in the standard sea ice formation scheme, sea ice forms instantly in response to ocean surface supercooling, it may take several model timesteps for new sea ice to form when the grease scheme is implemented. This, and the non-uniform thickness distribution of grease ice (following herding by the wind against sea ice edges), which may freeze to form a non-uniform distribution of sea ice, means that areas of open water persist for longer when the grease scheme is implemented, prolonging the ocean's exposure to atmospheric cooling and driving increased frazil ice production. This increased frazil production drives an increase in Arctic sea ice volume. In the standard sea ice formation scheme, the frazil ice is considered to be sea ice, whereas in the new scheme presented here, it forms grease ice, which may be transported from the supercooling location before freezing to form new sea ice.

In both hemispheres, implementing the grease scheme results in some local redistribution of sea ice. In general, new sea ice in areas of partial ice cover is thicker when the grease scheme is implemented, following herding of the grease ice against the sea ice edge, and the lateral growth of new sea ice to close leads 'from the sides' (rather than forming a cap across the upper surface of the lead). This means that new sea ice may be as thick as any existing sea ice in partially ice-covered grid cells. This thickening effect is greater in the Arctic, where sea ice is generally thicker, than in the Antarctic, although the grease scheme does drive a thickening of summer sea ice in coastal areas in the Antarctic.

In the Antarctic, changes in winter concentration, and to a lesser extent thickness, are associated with the production of grease ice, rather than sea ice, in polynya regions. The increased surface cooling when the grease scheme is implemented drives an increase in both sea ice concentration and thickness in the Western Pacific, as grease ice is transported away from the areas of supercooling at the coast and freezes into the ice pack, leaving the polynya surfaces exposed to further cooling and further frazil production. In the Amundsen Sea, grease ice forms in an area of convection relatively close to the northern ice edge, and is transported northwards to where it melts without ever having frozen to form new sea ice. In the Amundsen Sea, there is a therefore a decrease in the sea ice concentration and thickness when the grease scheme is implemented. These two regions dominate the sea ice response to the grease scheme in the Antarctic and are of roughly equal magnitude, leaving little net change to total Antarctic sea ice volume.

We have shown that the implementation of a more detailed sea ice formation scheme results in some changes to the spatial distribution of sea ice, particularly in the Antarctic winter, but no change to the total area in either summer or winter in either hemisphere. Including grease ice drives an increase in volume and thickness for simulated Arctic sea ice, and causes local changes (thinning and thickening) to simulated Antarctic sea ice. Sea ice volume represents latent heat and so is important to the energy balance of the ocean, but is difficult to estimate from observations because it requires reliable measurements of sea ice thickness with wide spatial coverage. This makes it particularly important that models include appropriately detailed physics in order to calculate reliable sea ice volume estimates.

The grease scheme presented here makes the representation of sea ice formation more physically realistic. This implementation contains some necessary assumptions which previous works have shown are likely to impact the results. More observations of grease ice properties would allow these assumptions to be better constrained in future. More observations of sea ice thickness are also needed, particularly in the Antarctic, to guide model development work and to assess model biases in simulated sea ice volume.

The scale of the increase in Arctic sea ice thickness and volume demonstrates that grease ice formation is a relevant and important process for climate simulations. Although in this work the thickening effect does not lead to an improved (more realistic) thickness because HadGEM3-GC3.1 overestimates historical Arctic sea ice, this is connected to the cold bias in the historical simulations, and should not be interpreted to mean that the processes leading to increased ice growth are unrealistic. The state of sea ice in a climate model depends on the interaction of all model components and therefore the implementation of a new process, such as grease ice formation, generally requires further tuning steps for the other model components. The changes seen here to result from the inclusion of grease ice processes in the model, including increased thermodynamic growth in areas where there is high ice divergence and/or thick partial ice cover, local effects such as those seen in the Amundsen Sea, and greater differences between seasonal and multiyear ice thicknesses, provide a more realistic description of sea ice in those areas, and this can be used to inform appropriate tuning for other processes in the model.

Appendix A Timeseries of Total Sea Ice Area

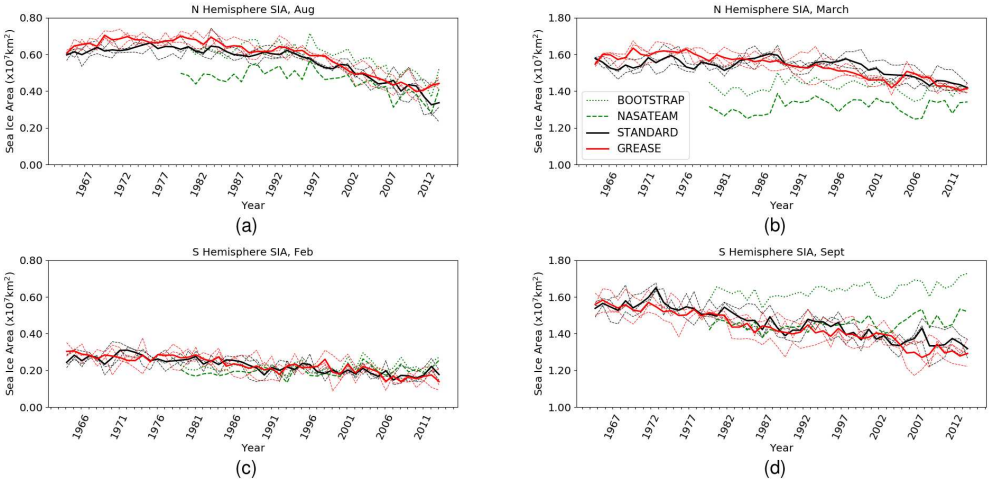

Figure A1. Total sea ice area. Ensemble means for GREASE and STANDARD are in bold, dashed lines are individual ensemble members. (a) August, Arctic; (b) March, Arctic; (c) February, Antarctic; (d) September, Antarctic. Note the different scales for summer and winter.

Acknowledgments

This work was funded by New Zealand Deep South National Science Challenge, Targeted Observations and Process-informed Modelling of Antarctic Sea Ice, contract C01X1445. Data for STANDARD were provided by U.K. Met Office and we acknowledge use of the Monsoon2 system, a collaborative High Performance Computing facility funded by the Met Office and the Natural Environment Research Council. PJL, DS & DF enjoyed support and hospitality from the Isaac Newton Institute for Mathematical Sciences, Cambridge during the Mathematics of Sea Ice Phenomena, EPSRC grant no EP/K032208/1. The data analysed in this work are large, requiring in excess of 100 GB of storage. They are therefore not included with this manuscript as supporting information, but can be shared with reviewers on request. The data are are currently being uploaded to the PANGAEA repository, where they will be available under a creative commons licence, and we will inform the JAMES editorial team once this is complete and add the citation to this statement.

References

Arrigo, K. R., Robinson, D. H., Worthen, D. L., Dunbar, R. B., DiTullio, G. R., VanWoert, M., & Lizotte, M. P. (1999). Phytoplankton community structure and the drawdown of nutrients and CO2 in the Southern Ocean. *Science*, *283*(5400), 365–367. doi: 10.1126/science.283.5400.365

Cavalieri, D. J., Parkinson, C. L., Gloersen, P., & Zwally, H. J. (1996). *Sea ice concentrations from Nimbus-7 SMMR and DMSP SSM/I-SSMIS passive microwave data, Version 1, updated yearly.* NASA National Snow and Ice Data Center Distributed Active Archive Center. (accessed 16 January 2010) doi: https://doi.org/10.5067/8GQ8LZQVL0VL

Comiso, J. (2017). *Bootstrap sea ice concentrations from Nimbus-7 SMMR and DMSP SSM/I-SSMIS, Version 3.* NASA National Snow and Ice Data Center Distributed Active Archive Center. (accessed 16 January 2010) doi: https://doi.org/10.5067/7Q8HCCWS4I0R

Dai, M., Shen, H. H., Hopkins, M. A., & Ackley, S. F. (2004). Wave rafting and the equilibrium pancake ice cover thickness. *Journal of Geophysical Research: Oceans*, *109*(C7). doi: 10.1029/2003JC002192

Eyring, V., Bony, S., Meehl, G. A., Senior, C. A., Stevens, B., Stouffer, R. J., & Taylor, K. E. (2016). Overview of the Coupled Model Intercomparison Project phase 6 (CMIP6) experimental design and organization. *Geoscientific Model Development*, *9*(5), 1937–1958. Retrieved from `https://www.geosci-model-dev.net/9/1937/2016/` doi: 10.5194/gmd-9-1937-2016

Heorton, H. D. B. S., Radia, N., & Feltham, D. L. (2017). A model of sea ice formation in leads and polynyas. *Journal of Physical Oceanography*, *47*(7), 1701-1718. doi: 10.1175/JPO-D-16-0224.1

Holland, P. R., & Kwok, R. (2012, Nov 11). Wind-driven trends in Antarctic sea-ice drift. *Nature Geoscience*, *5*, 872 EP -. Retrieved from `https://doi.org/10.1038/ngeo1627`

Hunke, E. C., Lipscomb, W. H., Turner, A. K., Jeffrey, N., & Elliott, S. (2015). *CICE: the Los Alamos sea ice model documentation and software users manual version 5.1, LA-CC-06-012* (Tech. Rep.). Los Alamos National Laboratory, Los Alamos NM 87545.

Kuhlbrodt, T., Jones, C. G., Sellar, A., Storkey, D., Blockley, E., Stringer, M., ... Walton, J. (2018, 11). The lowresolution version of HadGEM3 GC3.1: Development and evaluation for global climate. *Journal of Advances in Modeling Earth Systems*. Retrieved from `https://doi.org/10.1029/2018MS001370` doi: 10.1029/2018MS001370

Lambe, T., & Whitman, R. (1979). *Soil mechanics, SI version*. Wiley. Retrieved from `https://books.google.co.nz/books?id=CvpRAAAAMAAJ`

Langehaug, H., Geyer, F., Smedsrud, L., & Gao, Y. (2013). Arctic sea ice decline and ice export in the CMIP5 historical simulations. *Ocean Modelling*, *71*, 114 - 126. (Arctic Ocean) doi: https://doi.org/10.1016/j.ocemod.2012.12.006

Lewis, E. L., & Perkin, R. G. (1983). Supercooling and energy exchange near the Arctic Ocean surface. *Journal of Geophysical Research: Oceans*, *88*(C12), 7681-7685. doi: 10.1029/JC088iC12p07681

Lewis, E. L., & Perkin, R. G. (1986). Ice pumps and their rates. *Journal of Geophysical Research: Oceans*, *91*(C10), 11756-11762. Retrieved from `https://agupubs.onlinelibrary.wiley.com/doi/abs/10.1029/JC091iC10p11756` doi: 10.1029/JC091iC10p11756

Madec, G., & team, N. (2016). *NEMO ocean engine, version 3.6 stable* (Vol. 27; Tech. Rep.). Pole de modelisation de lInstitut Pierre-Simon Laplace.

Martin, S., & Kauffman, P. (1981). A field and laboratory study of wave damping by grease ice. *Journal of Glaciology*, *27*(96), 283313. doi: 10.3189/S0022143000015392

Maus, S., & De La Rosa, S. (2012). Salinity and solid fraction of frazil and grease ice. *Journal of Glaciology*, *58*(209), 594612. doi: 10.3189/2012JoG11J110

Menary, M. B., Kuhlbrodt, T., Ridley, J., Andrews, M. B., Dimdore-Miles, O. B., Deshayes, J., ... Xavier, P. (2018). Preindustrial control simulations with HadGEM3-GC3.1 for CMIP6. *Journal of Advances in Modeling Earth Systems*, *10*(12), 3049-3075. doi: 10.1029/2018MS001495

Morales Maqueda, M. A., Willmott, A. J., & Biggs, N. R. T. (2004). Polynya dynamics: a review of observations and modeling. *Reviews of Geophysics*, *42*(1). doi: 10.1029/2002RG000116

Pauling, A. G., Smith, I. J., Langhorne, P. J., & Bitz, C. M. (2017). Time-dependent freshwater input from ice shelves: Impacts on Antarctic sea ice and the Southern ocean in an Earth System Model. *Geophysical Research Letters*, *44*(20), 10,454-10,461. doi: 10.1002/2017GL075017

Ridley, J. K., Blockley, E. W., Keen, A. B., Rae, J. G. L., West, A. E., & Schroeder, D. (2018). The sea ice model component of HadGEM3-GC3.1. *Geo-*

scientific Model Development, *11*(2), 713-723. Retrieved from https://www.geosci-model-dev.net/11/713/2018/ doi: 10.5194/gmd-11-713-2018

Schweiger, A., Lindsay, R., Zhang, J., Steele, M., Stern, H., & Kwok, R. (2011). Uncertainty in modeled Arctic sea ice volume. *Journal of Geophysical Research: Oceans*, *116*(C8). Retrieved from https://agupubs.onlinelibrary.wiley.com/doi/abs/10.1029/2011JC007084 doi: 10.1029/2011JC007084

Shu, Q., Song, Z., & Qiao, F. (2015). Assessment of sea ice simulations in the CMIP5 models. *The Cryosphere*, *9*(1), 399–409. Retrieved from https://www.the-cryosphere.net/9/399/2015/ doi: 10.5194/tc-9-399-2015

Skogseth, R., Nilsen, F., & Smedsrud, L. H. (2009). Supercooled water in an Arctic polynya: observations and modeling. *Journal of Glaciology*, *55*(189), 4352. doi: 10.3189/002214309788608840

Smedsrud, L. H. (2011). Grease-ice thickness parameterization. *Annals of Glaciology*, *52*(57), 7782. doi: 10.3189/172756411795931840

Smedsrud, L. H., & Martin, T. (2015). Grease ice in basin-scale sea-ice ocean models. *Annals of Glaciology*, *56*(69), 295306. doi: 10.3189/2015AoG69A765

Smedsrud, L. H., & Skogseth, R. (2006). Field measurements of arctic grease ice properties and processes. *Cold Regions Science and Technology*, *44*, 171-183. doi: 10.1016/j.coldregions.2005.11.002

Stirling, I. (1997). The importance of polynyas, ice edges, and leads to marine mammals and birds. *Journal of Marine Systems*, *10*(1), 9 - 21. doi: https://doi.org/10.1016/S0924-7963(96)00054-1

Storkey, D., Blaker, A. T., Mathiot, P., Megann, A., Aksenov, Y., Blockley, E. W., ... Sinha, B. (2018). UK Global Ocean GO6 and GO7: a traceable hierarchy of model resolutions. *Geoscientific Model Development*, *11*(8), 3187–3213. Retrieved from https://www.geosci-model-dev.net/11/3187/2018/ doi: 10.5194/gmd-11-3187-2018

Stroeve, J., Barrett, A., Serreze, M., & Schweiger, A. (2014). Using records from submarine, aircraft and satellites to evaluate climate model simulations of Arctic sea ice thickness. *The Cryosphere*, *8*(5), 1839–1854. Retrieved from https://www.the-cryosphere.net/8/1839/2014/ doi: 10.5194/tc-8-1839-2014

Turner, J., Bracegirdle, T. J., Phillips, T., Marshall, G. J., & Hosking, J. S. (2013). An initial assessment of Antarctic sea ice extent in the CMIP5 models. *Journal of Climate*, *26*(5), 1473-1484. doi: 10.1175/JCLI-D-12-00068.1

Walters, D., Baran, A. J., Boutle, I., Brooks, M., Earnshaw, P., Edwards, J., ... Zerroukat, M. (2019). The Met Office Unified Model Global Atmosphere 7.0/7.1 and JULES Global Land 7.0 configurations. *Geoscientific Model Development*, *12*(5), 1909–1963. Retrieved from https://www.geosci-model-dev.net/12/1909/2019/ doi: 10.5194/gmd-12-1909-2019

Wang, X., Key, J., Kwok, R., & Zhang, J. (2016). Comparison of Artcic sea ice thickness from satellites, aircraft and PIOMAS data. *Remote Sensing*, *8*. doi: 10.3390/rs8090713

Weeks, W. (2010). *On sea ice*. University of Alaska Press. Retrieved from https://books.google.co.nz/books?id=9S55O6WzuL8C

Wilchinsky, A. V., Heorton, H. D. B. S., Feltham, D. L., & Holland, P. R. (2015). Study of the impact of ice formation in leads upon the sea ice pack mass balance using a new frazil and grease ice parameterization. *Journal of Physical Oceanography*, *45*(8), 2025-2047. doi: 10.1175/JPO-D-14-0184.1

Williams, K. D., Copsey, D., Blockley, E. W., Bodas-Salcedo, A., Calvert, D., Comer, R., ... Xavier, P. K. (2017). The Met Office Global Coupled Model 3.0 and 3.1 (GC3.0 and GC3.1) configurations. *Journal of Advances in Modeling Earth Systems*, *10*(2), 357-380. doi: 10.1002/2017MS001115

Winsor, P., & Björk, G. (2000). Polynya activity in the Arctic Ocean from 1958 to 1997. *Journal of Geophysical Research: Oceans*, *105*(C4), 8789-8803. doi: 10

.1029/1999JC900305

Zhang, J., & Rothrock, D. A. (2003). Modeling global sea ice with a thickness and enthalpy distribution model in generalized curvilinear coordinates. *Monthly Weather Review*, *131*(5), 845-861. doi: 10.1175/1520-0493(2003)131⟨0845:MGSIWA⟩2.0.CO;2

Zunz, V., Goosse, H., & Massonnet, F. (2013). How does internal variability influence the ability of CMIP5 models to reproduce the recent trend in Southern Ocean sea ice extent? *The Cryosphere*, *7*(2), 451–468. Retrieved from `https://www.the-cryosphere.net/7/451/2013/` doi: 10.5194/tc-7-451-2013